Journal of Power Sources 663 (2026) 238931

Contents lists available at ScienceDirect

Journal of Power Sources

journal homepage: www.elsevier.com/locate/jpowsour

Structural behaviour and electrochemical study of V^{5+} based $LiTi_2(PO_4)_3$ solid electrolyte material for lithium-ion batteries

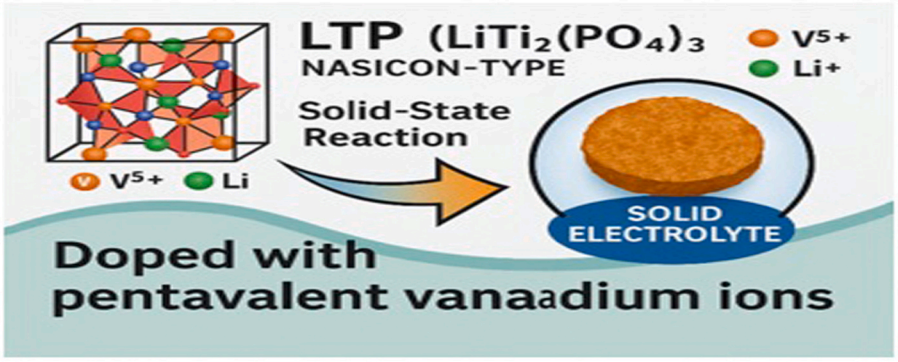
A. Panneerselvam [a,*], V.M. Senthilkumar [b], R. Senthil kumar [c], S. Satheeskumar [d], S. Selvakumar [e], S.C. Vella Durai [f]

[a] Department of Physics, Vivekanandha College of Engineering for Women (Autonomous), Tiruchengode, Namakkal, 637 205, Tamil Nadu, India
[b] Department of Electronics Engineering (VLSI Design and Technology), Rajalakshmi Institute of Technology, Chennai, Tamil Nadu, India
[c] Department of Physics, T.J.S. Engineering College, Peruvoyal, 601 206, Tamil Nadu, India
[d] Centre for Nanoscience and Technology, KS Rangasamy College of Technology, Tiruchengode, 637 215, Tamilnadu, India
[e] Department of Science and Humanities, Thamirabharani Engineering College (Autonomous), Thatchanallur, Tirunelveli, 627 358, Tamil Nadu, India
[f] P.G. and Research Department of Physics, Sri Paramakalyani College, Alwarkurichi, Tenkasi, 627 412, Tamil Nadu, India

HIGHLIGHTS

- Vanadium doping in $LiTi_2(PO_4)_3$ enhances Li^+ conductivity to 0.82×10^{-4} S/cm at room temperature.
- Incorporation of V^{5+} ions alters the lattice, widening ion pathways and improving Li^+ mobility.
- The composition $Li_{1-x}(PO_4)_3$ (x = 0.15) shows maximum conductivity, emphasizing the importance of precise doping control.
- V-doped LTP proves to be a promising solid electrolyte with excellent stability and high ionic conductivity at low temperatures.

GRAPHICAL ABSTRACT



ARTICLE INFO

Keywords:
Vanadium based LTP
Solid electrolytes
Pentavalent cation
High conductivity
Rhombohedral structure

ABSTRACT

This study investigates the effect of adding pentavalent vanadium ions to $LiTi_2(PO_4)_3$-based electrolytes to enhance ionic conductivity. Vanadium-doped samples with compositions $Li_{1-x}Ti_{2-x}V_{x3}$ (x = 0.05, 0.10, 0.15) were prepared via a solid-state method. XRD analysis confirmed the formation of a pure rhombohedral phase, while SEM showed particle sizes between 0.5 and 1 μm. Electrochemical impedance tests revealed the highest conductivity for x = 0.15. The doped electrolytes exhibited better structural stability and higher conductivity at temperatures from 150 °C to 350 °C compared to undoped samples. Doping widened the ion-conduction pathway, resulting in a Li-ion conductivity of 0.82×10^{-4} S/cm at room temperature. These findings demonstrate that incorporating pentavalent cations like vanadium into LTP electrolytes is an effective approach for improving performance, offering potential for advanced solid-state lithium batteries.

* Corresponding author.
E-mail address: panneer.phy@gmail.com (A. Panneerselvam).

https://doi.org/10.1016/j.jpowsour.2025.238931
Received 22 September 2025; Received in revised form 30 October 2025; Accepted 21 November 2025
0378-7753/© 2025 Elsevier B.V. All rights are reserved, including those for text and data mining, AI training, and similar technologies.

1. Introduction

Powering modern electronic devices and autonomous systems has become increasingly dependent on lithium-ion batteries (LIBs) because of their lightweight design, high output power, and superior energy density. However, most commercially available LIBs rely on liquid electrolytes and organic polymer separators, which present several limitations. These include poor oxidative stability, a high risk of flammability, and limited compatibility between lithium metal anodes and the electrolyte. To overcome these drawbacks, the replacement of liquid electrolytes with solid-state electrolytes has emerged as a promising solution. Inorganic solid electrolytes offer higher thermal stability, improved compatibility with lithium metal anodes, and enhanced ionic conductivity. Solid-state electrolytes cover a broad range of materials, including organic polymers, inorganic compounds such as oxides and sulphides, and composite systems that combine polymer [poly(vinylidene fluoride)] and ceramic [$Li_4Ti_5O_{12}$] electrolytes [1–5]. In recent decades, various types of inorganic oxide electrolytes have been extensively studied, including perovskite-type ($Li_{3+x}La_{2/3-x}TiO_3$, LLTO), NASICON-type ($Li_{1+x}Y_xZr_{2-x}(PO_4)_3$, LYZP) and ($Li_{1+x}Al_xGe_{2-x}(PO_4)_3$, LAGP) systems, as well as garnet-type ($Li_7La_3Zr_2O_{12}$, LLZO). In addition, sulphide-based systems such as argyrodite-type (Li_6PS_5Cl) and thiophosphate-type (Li_3PS_4, e.g., $Li_{10}GeP_2S_{12}$, LGPS) solid electrolytes have also received considerable attention [6–9]. Among these, NASICON-type oxide materials with a rhombohedral *R*3*c* structure are particularly noteworthy due to their three-dimensional ion transport framework. Since the early 1990s, compounds such as $LiTi_2(PO_4)_3$ (LTP) have been widely investigated for lithium-ion conduction. However, the ionic conductivity of LTP remains lower than that of liquid electrolytes, despite the presence of multiple diffusion pathways, indicating the need for further improvement.

Doping is a well-established method to modify the electrochemical properties of electrolytes, where aliovalent substitution is used to increase the concentration of charge-carrying defect species. Replacing Ti^{4+} with aliovalent cations such as Ca^{2+} or Al^{3+} can effectively tune the ionic conductivity of LTP, while isovalent doping with cations like Hf^{4+} can also influence its transport behavior. Additionally, introducing pentavalent elements such as vanadium or niobium at the tetrahedral sites can further enhance ionic conductivity. Among these dopants, Al^{3+} substitution has shown remarkable efficiency in improving lithium-ion transport, as demonstrated in the $Li_{1+x}Al_xTi_{2-x}(PO_4)_3$ (LATP) system.

The substitution notably alters the cell volume and simultaneously weakens the Li–O bond strength. Furthermore, the incorporation of Al^{3+} results in the formation of an impurity phase containing aluminum-rich $AlPO_4$, which enhances densification and contributes positively to composite formation, thereby improving the overall ionic conductivity. However, when the Al concentration increases, adverse effects become more pronounced, such as a significant accumulation of residual lithium on the cathode surface and a reduction in the initial capacity. These drawbacks arise due to the generation of impurity phases like $LiAlO_2$ and Li_5AlO_4. In addition, a higher grain boundary impedance in LATP leads to reduced overall performance.

Some research articles proposed that the presence of impurities at grain boundaries leads to the formation of a space-charge region, which intensifies with increasing dopant (Sc_{3+}, Y_{3+}) concentration. Electrochemical impedance studies have shown that this space charge formation correlates with an increased diffusion coefficient and mean square displacement. Consequently, for advanced electrochemical energy storage systems, NASICON-type LTP-based solid electrolytes have drawn significant scientific attention as promising inorganic solid-state electrolytes (SSEs).

Among lithium-ion conductors with NASICON structures – such as $LiTi_2(PO_4)_3$ (LTP), $Li_{1.3}Al_{0.3}Ti_{1.7}(PO_4)_3$ (LATP), $LiSnZr(PO_4)_3$, $Li_{1.5}Al_{0.5}Ge_{1.5}(PO_4)_3$, and $Li_{1+x}Cr_xTi_{2-x}(PO_4)_3$ .remarkable ionic conductivities ranging from 10^{-3} to 10^{-4} Ω^{-1} cm^{-1} at room temperature have been reported. This behavior is attributed to the unique three-dimensional framework of PO_4 tetrahedra corner-shared with MO_6 octahedra, which forms continuous pathways for lithium-ion migration [10–15]. As a result, Li^+ - NASICONs are recognized as strong candidates for solid electrolytes in all-solid-state lithium-ion batteries (ASSBs).

In addition to their role as electrolytes, NASICON-structured mixed ionic systems have also been studied as potential electrode and cathode materials. For instance, Some research articles reported a NASICON-type compound, $Li_3Fe_2(PO_4)_3$, which exhibited an electrochemical potential of approximately 2.8 V versus Li/Li^+ [16–19]. Similarly, Some research articles reported a synthesized $Li_3V_2(PO_4)_3$ for use as a cathode in battery applications. Several studies have also explored vanadium-substituted $Li_{1.3}Al_{0.3}Ti_{1.7}(PO_4)_{2.9}V_{0.1}$ (LATPV), where partial substitution of V^{5+} for P^{5+} slightly enhanced conductivity while significantly improving thermal stability and density.

The improved electronic conductivity in NASICON-type materials originates from transition metal–oxygen bonds, leading to mixed ionic–electronic (MIE) transport due to the substantial presence of transition metal oxides. Such MIE systems are applicable not only in batteries but also in supercapacitor electrodes and high-current discharge devices requiring rapid electron transfer. Achieving high power density further demands fast cation insertion and extraction from the electrode lattice. Transition metal oxides like RuO_2, TiS_2, and Fe_3O_4 have been widely examined for their superior electronic conductivity and quick electron transfer characteristics.

Incorporating electronic conduction into LTP-based glass–ceramic composites has led to the development of MIE glass–ceramic materials suitable for cathode and electrode applications, as demonstrated in recent studies. In this work, MIE glass was introduced externally in small proportions into the Li^+ - NASICON matrix, and subsequent heat treatment yielded innovative MIE glass–ceramics. These LTP-based composites displayed a total conductivity of approximately 0.92×10^{-2} cm^{-1} at 350 °C, with activation energy of about 0.25 eV. The LTP grains enabled pure ionic transport, while the MIE glass at the grain interfaces facilitated electronic transport within the composite.

Enhanced ion intercalation and improved electronic conductivity are essential for efficient electrode and cathode performance. Alternatively, electronic conduction can also be achieved directly by substituting suitable transition metals into the Li^+ - NASICON lattice to enable long-range mixed ionic–electronic transport [20–22]. Hence, this study focuses on the substantial substitution of vanadium to promote electronic conduction in $LiTi_2(PO_4)_3$ (LTP) matrices. Detailed investigations on the structural and electronic transport properties were carried out for various vanadium concentrations in NASICON-type LTP matrices, with emphasis on their potential applications as solid electrolytes for lithium-ion batteries and energy storage systems.

2. Experimental

2.1. Synthesis process

For this study, vanadium-doped LTP, specifically $LiTi_2(PO_4)_{3-x}(VO_4)_x$ with x ranging from 0.05, 0.10 and 0.15, were synthesized using a solid-state reaction method from a stoichiometric blend of Li_2NO_3, TiO_2, $NH_4H_2PO_4$ and V_2O_5. These mixtures were subjected to annealing at 800 °C for 2 h, followed by an additional annealing at 1150 °C for another 2 h. After annealing, the mixture was pelletized with a hydraulic press, applying a pressure of 4 tons/cm^2 for 15 min. The formed composite pellets were subsequently annealed at 900 °C for 30 min and allowed to cool in the furnace. No significant cracks were detected on the pellets. The surfaces of the pellets were polished to achieve smoothness. The resulting composites were designated as LVTP - (where x - 0.05, 0.10 & 0.15).

2.2. Characterizations

To structurally characterize the samples, a powder X-ray

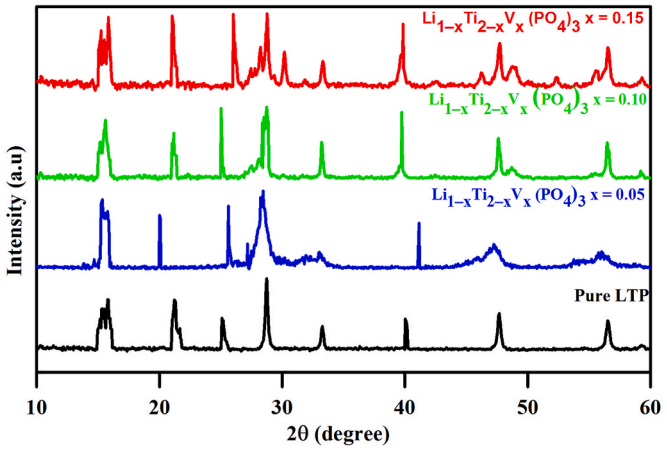


Fig. 1. XRD patterns of the prepared LTP and V doped LTP (x = 0.05, 010 and 0.15) powder electrolyte samples.

Table 1
Lattice parameters of the prepared LTP and V doped LTP (x = 0.05, 0.10 and 0.15) sample powders.

	a (Å)	c(Å)	c/a
LTP x = 0	8· 6125	20·9604	2·5412
LVTP x = 0.05	8· 6102	20·9483	2·5383
LVTP x = 0.10	8· 614	20·9223	2·5408
LVTP x = 0.15	8· 6003	20·9635	2·5676

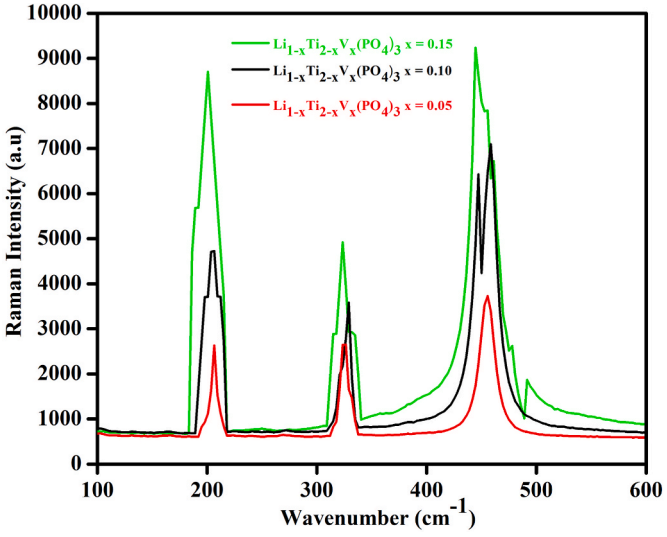


Fig. 2. Raman spectra of $Li_{1-x}Ti_{2-x}V_x$ $(PO_4)_3$ sintered powders.

diffractometer (Bruker D8 Advance equipped with CuKα radiation) was utilized. High temperature X-ray diffraction measurements were performed in situ using the Bruker D8 Advance equipped with CuKα radiation X-ray diffractometer to investigate structural stability at elevated temperatures. Both X-ray diffractometers operated with CuKα radiation (1.54 Å). The surface morphology of the samples was examined through scanning electron microscopy (SEM) TESCAN VEGA3 LMU instrument. Raman spectra were obtained using a WITEC ALPHA 300-R instrument utilizing a 532 nm source wavelength within the frequency range of 100–600 cm^{-1}. Ionic conductivity assessments were conducted on pellets measuring 12 mm in diameter and 1.5–2.5 mm in thickness, with measurements taken using a Biologic electrochemical workstation (Biologic VSP300) across a frequency range from 50 Hz to 1 MHz and a temperature range from 150 – 350° C.

3. Results and discussion

3.1. X-ray diffraction

The XRD patterns for LVTP-0.05, LVTP-0.10, LVTP-0.15, and LTP are presented in Fig. 1. It is clearly indicating that substitution does not disrupt the NASICON-type structure, on its observable that all the peaks in both LTP and LVTP remain intact even after significant V^{5+} doping,. However, there is a minor precipitation of a compound identified as V_3O_5 within the LTP matrix. Due to the substantial precipitation of V_3O_5 the compositions exceeding x = 0.15 for LTP were not considered. As shown, the peaks associated with the V^{5+} doped samples exhibit a trend similar to that of the pristine samples of LTP [23–26]. No phase separation or sudden precipitation of any compound is observed, across a broad temperature range. As the temperature changes, only the peaks related to the V_3O_5 compound are visible across the material, with its area remaining almost constant. It can be readily inferred that the V^{5+} doped samples maintain structural stability compared to that of the pristine samples. UNIT CELL fitting software, using LTP (card no: 35–0754) as a reference, the lattice parameters for the V doped samples were obtained as listed in Table 1.

As per calculations and measurements, the lattice parameters and unit cell volume show an observable decrease as the concentration of vanadium increases. Regardless, a systematic increase with temperature is seen in the unit cell volume for the V_{5+} doped samples. The XRD patterns of Li_{1-x} $[Ti_{2-x}V_x]$ $(PO_4)_3$ powders, which were sintered for 2 h at 1150 °C, are illustrated in Fig. 1. The XRD pattern obtained at this temperature corresponds to phase-pure compounds exhibiting a rhombohedral structure, and all detected peaks can be indexed according to JCPDS Card No. 35–0754 ($LiTi_2(PO_4)_3$). The phase presented in Fig. 1 aligns with the XRD pattern for LTP, indicating the creation of single-phase compounds. The unit cell parameters have been calculated utilizing UNITCELL software, 1995 with the results displayed in Table 1. The lattice parameters for LTP, derived from XRD data and presented in Table 1, are consistent with previously published crystallographic data. It is noted that the lattice parameters decrease as the x value in LTP increases, with the exception of x = 0.05. A corresponding peak shift for (113) is observed, as indicated in Fig. 1. Additionally, from Table 1 and it is noted that the experimental densities rise with increasing dopant concentration in LTP.

3.2. Raman spectra

The Raman spectra for LTP and vanadium-doped LTP samples are presented in Fig. 2, revealing the presence of three prominent symmetric stretching modes at 473, 466, and 451 cm^{-1}, alongside two antisymmetric stretching modes at 372 and 355 cm^{-1}. The peak observed at 325 cm^{-1} corresponds to the symmetric stretching mode of $(PO_3)_{4-}$, while the peaks at 231 and 222 cm^{-1} are attributed to the symmetric bending modes. The bands located below 209 cm^{-1} are associated with external modes, which are challenging to assign due to their mixing. The substitution of vanadium into LTP resulted in notable alterations in the asymmetric stretching modes. All the prominent peaks experienced a slight shift towards lower wavenumbers, accompanied by a reduction in intensity of the peaks at 492 and 486 cm^{-1}, which is linked to local disorder around the $(PO_3)_{4-}$ ions as vanadium is introduced into the titanium site of LTP [27–29].

3.3. Scanning electron microscopy

To explore the microstructure of vanadium doped LTP electrolyte materials, SEM analysis was conducted on LVTP (x = 0.05, 0.10, 0.15) samples that were annealed at temperatures of about 1150 °C are displayed in Fig. 3. While the sintered materials show largely similar

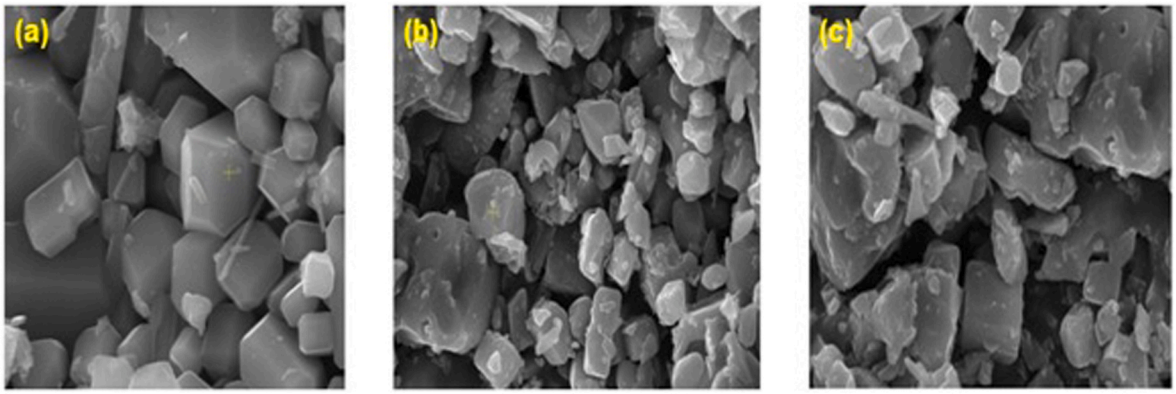


Fig. 3. (a, b, and c) SEM micrographs of LTP and V doped LTP (x = 0.05, 0.10 and 0.15) electrolyte samples.

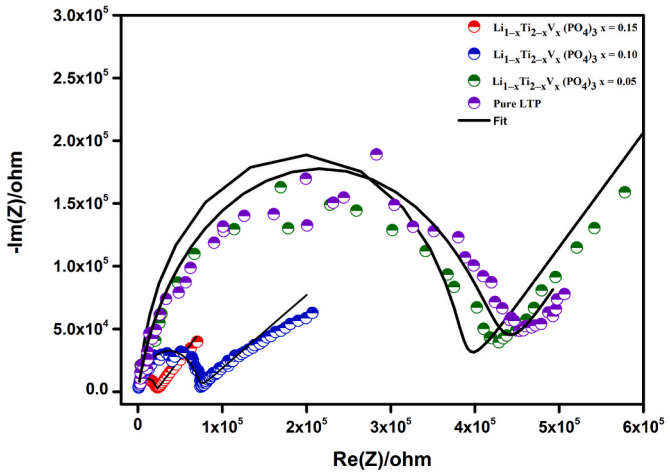


Fig. 4. Nyquist plots of LTP and V doped LTP (x = 0.05, 0.10 and 0.15) electrolyte measured at room temperature.

microstructures, there are notable differences. The undoped LTP sample features more spherical crystallites, whereas the LVTP samples possesses significantly more faceting and, particularly at 1150 °C, a marked increase in crystallite growth along with reduced porosity as in Fig. 3. The driving factors may include the (intermediate) production of lithium phosphate and the presence of $LiTiOPO_4$ as a sintering aid, attributed to their relatively low melting points. Overall, it can be concluded that the introduction of vanadium results in larger crystallite sizes. Fig. 3 presents SEM images of the fractured surfaces of pellets of LTP and vanadium-doped LTP that were sintered at 1150 °C for 2 h. The SEM micrographs reveal that the grain size substantially increased with the addition of vanadium content, alongside a certain degree of porosity. As observed, the submicron crystallites exhibit almost uniform sizes and a square texture. A closer look at the SEM images reveals a tendency for larger grain sizes across the samples. This increase in grain size is linked to the formation of bigger clusters, aided by the extensive surface area available from the smaller crystallites. Smaller crystalline particles generally possess a greater surface area to volume ratio, facilitating the creation of larger aggregates as they connect and interact more efficiently with one another. The structure shown through scanning electron microscopy (SEM) distinctly illustrates a more uniform distribution of particle sizes within the material's porous framework. This consistency in particle size distribution is crucial, as it results in more dependable and predictable material properties, which are important for various applications like sensor technology, super capacitors and energy storage systems. Additionally, the particle surfaces seem to be densely packed. This tight configuration is not merely a structural characteristic but also significantly influences the material's performance. Specifically, a closely packed surface morphology enhances the efficacy of charge carrier separation. Improved charge carrier separation is advantageous in several fields, particularly in solar energy and photocatalytic applications. To sum up, the SEM images provide a comprehensive view of the microscopic structure of the samples. The heightened interconnectivity among particles, the development of larger grains due to increased cluster formation, the more consistent particle size distribution, and the compact surface morphology all contribute to the material's improved properties.

3.4. EIS analysis

To assess the electrical transport properties, Nyquist plots for the various LVTP composites fitted with its corresponding equivalent circuit are presented in Fig. 4 at room temperature. Accompanied by a tail-like behavior at lower frequencies, a distinct broad and depressed semicircle is observed. These depressed semicircles often indicate a spectrum of relaxation times. A low-frequency tail is particularly noticeable in samples with low V^{5+} content, which gradually diminishes as the content in the matrix increases. The Nyquist plots for LVTP (x = 0.05, 0.10 & 0.15) at various operating temperatures are also displayed in Fig. 5, showing a depressed semicircle without any spur or inclined line at lower frequencies. In both instances, the transport within the grain and across the grain boundary cannot be distinguished. Consequently, the total conductivity (σ_{total}) was extracted from the low-frequency intercept of the semicircles with the |Z'| axis. Two distinctly separated plateau regions are observed at low and high frequencies for LVTP. Meanwhile, LVTP with low V^{5+} content shows a single plateau. Notably, a transport behavior akin to LTP is evident when the V^{5+} content is reduced in the LTP matrix. For higher V^{5+} contents, only a single plateau region is apparent, suggesting long-range electrical transport along with a gradual decrease in conductivity as frequency lowers [30,31]. Unlike systems where ionic transport is predominant, this decline is not severe, implying mild polarization at the interface. Among all LVTP composites, LVTP - 0.15 displays the highest σ_{total} value (approximately 0.92×10^{-2} cm^{-1}) at 350 °C. Fig. 5 illustrates the frequency-dependent total conductivity across all LVTP samples. It can be observed that total conductivity consistently increases with rising V^{5+} content in LTP (as shown in Fig. 5. Similar to LVTP – 0.10, LTP - 0.15 shows the highest conductivity (about 0.19×10^{-3} and 0.92×10^{-2} cm^{-1} at 350 °C). The total conductivity values for LVTP – 0.05, 0.10 and 0.15 compositions are graphed against temperature (150, 250, and 350 °C) in Fig. 5(a and b and c), respectively. For the LTP-V composites, σ_{total} demonstrates a gradual increase with higher V^{5+} content in LTP. Although the activation energy values do not exhibit a specific trend with V^{5+} levels, they are generally lower than those of pristine LTP. Conversely, for LTP, an increase in V^{5+} content (up to x = 0.2) leads to a significant drop in

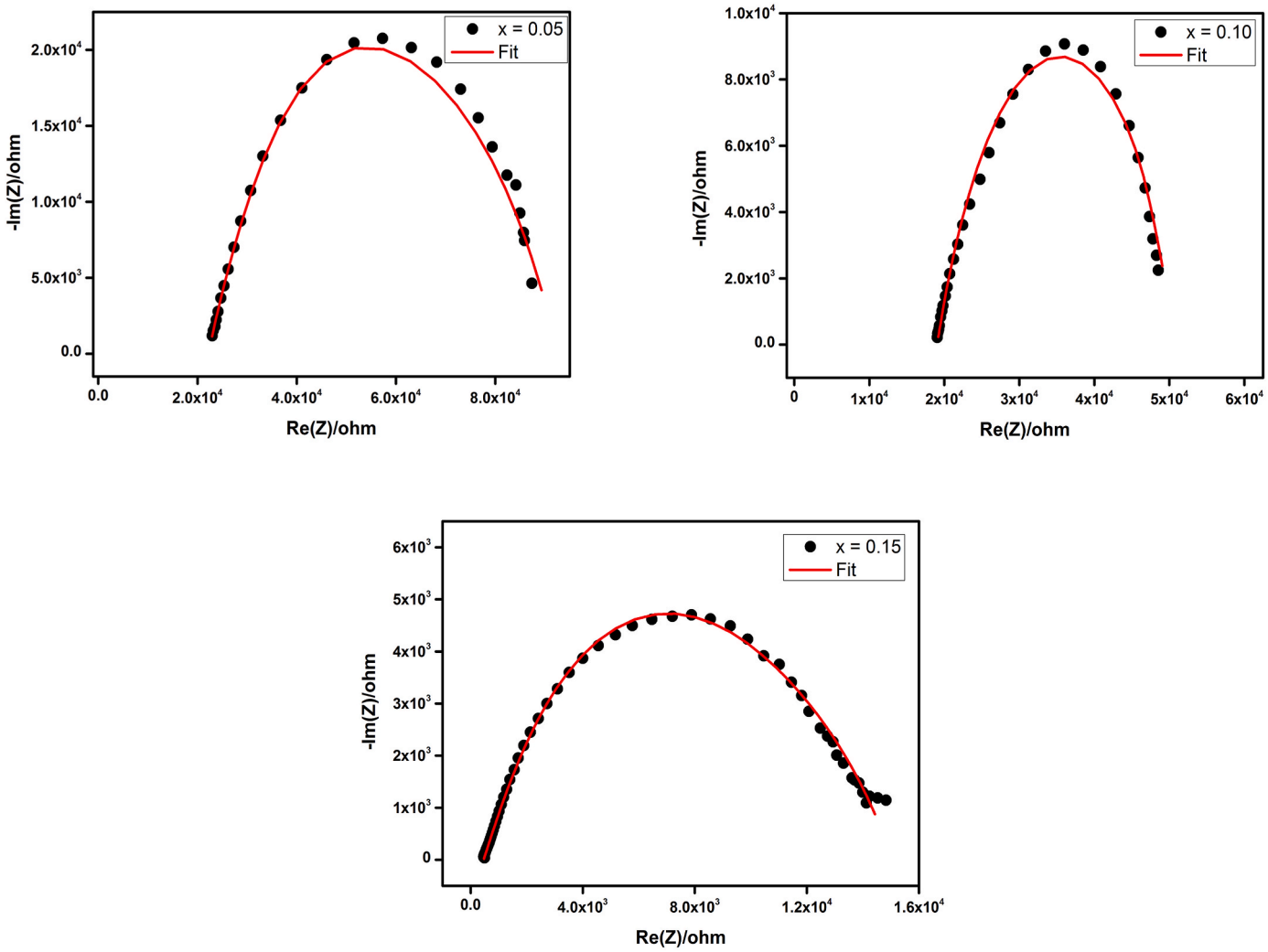


Fig. 5 (a). Nyquist plots of V doped LTP at x = 0.05, 0.10 and 0.15 electrolytes measured at 150° C operating temperature.

conductivity. Given the complexity of the LTP structure, some distortion in the 3D tunnels is anticipated due to V^{5+} substitution. While XRD does not indicate any significant lattice distortion, it is conceivable that at the molecular level, substitutions may disrupt Li^{+} ion sites, hindering electrical transport. With a further increase in V (x = 0.10–0.15), conductivity shows a systematic and marked increase. Additionally, the activation energy is observed to be for LVTP – 0.15 as 0.25 eV.

The ionic conductivities recorded for LVTP samples doped with vanadium at concentrations of x = 0.05, 0.1, and 0.15 are 0.59×10^{-5}, 0.27×10^{-5} and 0.82×10^{-4} S/cm, respectively, at room temperature.

However, all of the vanadium-doped samples exhibited higher ionic conductivity compared to the un doped LTP, which has a conductance of 0.71×10^{-5} S/cm. These findings indicate that the ionic conductivity is highest at x = 0.15 for vanadium-doped LTP. Table 2 presents the ionic conductivity values for both LTP and vanadium-doped LTP materials at room temperature. The data in this table reveal that ionic conductivity increases with both frequency and temperature for each composition. Fig. 6 illustrates the Arrhenius AC conductivity graphs for $Li_{1-x}Ti_{2-x}V_x(PO_4)_3$. It can be seen from the figure that ionic conductivity rises steadily from room temperature to elevated temperatures, as shown in Table 3. The plots of log σ against 1000/T K demonstrate a nearly linear relationship, adhering to the Arrhenius equation. The activation energies for a.c. conductivity across different temperature ranges were determined by measuring the slopes of the curves and applying the equation $\sigma = \sigma_0 \exp^{[-Ea/kT]}$, where σ_0 represents a pre-exponential factor, E_a is the activation energy, k denotes Boltzmann's constant, and T refers to absolute temperature. The activation energy value for the sample with higher ionic conduction was found to be 0.25 eV for vanadium-doped LTP samples at x = 0.15. The observed increase in ionic conductivity with V^{5+} substitution can be attributed to the creation of Li^{+} vacancies for charge balance and slight lattice distortion in the NASICON framework, which together broaden Li^{+} conduction pathways. The higher valence and radius of V^{5+} compared to Ti^{4+} induce structural relaxation that reduces the migration barrier, consistent with prior DFT-based reports on doped LTP systems. The enhancement of ionic conductivity in $Li_{1+x}V_xTi_{2-x}(PO_4)_3$ (x = 0.05, 0.10, 0.15) can be rationalized based on structural and defect chemistry considerations. The partial substitution of Ti^{4+} by aliovalent V^{5+} ions introduces charge imbalance in the NASICON framework, which is compensated by the generation of additional Li^{+} vacancies to preserve overall charge neutrality. These vacancies act as favorable sites for Li^{+} migration and effectively reduce the migration barrier. Moreover, the slightly larger ionic radius and higher valence of V^{5+} (0.54 Å) compared to Ti^{4+} (0.53 Å) lead to local lattice distortion and expansion of the Li–O conduction bottlenecks, thereby widening the diffusion channels for Li^{+} transport. This structural relaxation enhances the three-dimensional connectivity of Li^{+} migration pathways in the NASICON framework. Consequently, the ionic conductivity increases systematically with increasing vanadium content, reaching a maximum value of 0.82×10^{-4} S cm^{-1} at room temperature and 0.92×10^{-2} S cm^{-1} at 350 °C for the composition x =

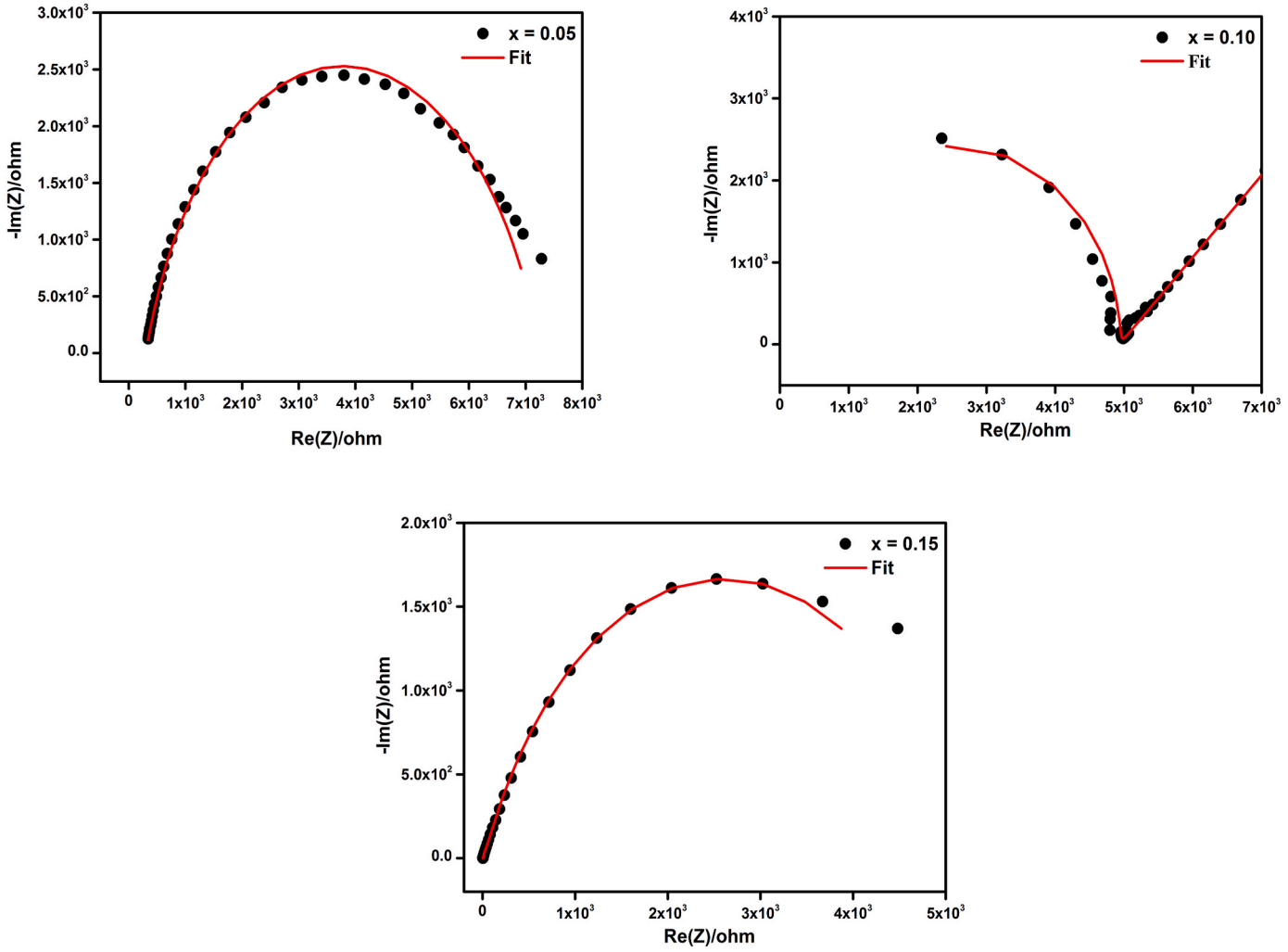


Fig. 5 (b). Nyquist plots of V doped LTP at x = 0.05, 0.10 and 0.15 electrolytes measured at 250° C operating temperature.

0.15. This improvement corroborates the proposed mechanism of defect-assisted ion migration. The observed behavior is consistent with earlier DFT and molecular dynamics studies on aliovalent doping in NASICON-type electrolytes, where lattice distortion and Li^+ vacancy formation were shown to broaden diffusion pathways and lower activation energy barriers for ion transport [32,33].

The substitution of pentavalent vanadium ions (V^{5+}) into the $LiTi_2(PO_4)_3$ lattice significantly enhances both the structural and electrochemical performance of the material (Fig. 7). The V^{5+} incorporation partially replaces Ti^{4+} in the NASICON framework, introducing a charge imbalance that promotes the creation of additional lithium vacancies and facilitates faster Li^+ ion transport. This structural modification leads to an improved ionic conductivity of 0.82×10^4 S/cm at room temperature and 0.92×10^2 S/cm at 350 °C, which is markedly higher than that of undoped LTP. Additionally, vanadium substitution enhances the crystallinity and stabilizes the NASICON phase, as confirmed by XRD and SEM analyses. The improved microstructural uniformity and reduced grain boundary resistance further contribute to enhanced ion migration. From an electrochemical perspective, the V^{5+} ions not only improve the lattice dynamics but also extend the material's electrochemical stability window, making it suitable for high-temperature and high-voltage lithium-ion battery applications. Vanadium-substituted LTP exhibits exceptional properties, making it a promising material for solid-state electrolytes. Its standout features include enhanced ionic conductivity resulting from increased Li^+ mobility pathways, improved phase stability, and structural robustness due to substitution. The material also demonstrates reduced grain boundary resistance, leading to superior electrochemical kinetics. Furthermore, it boasts high thermal and chemical stability, ensuring reliable performance under operating conditions. Notably, its relatively simple synthesis process compared to other high-conductivity solid electrolytes adds to its appeal.

4. Conclusion

Powders with various compositions of $Li_{1-x}Ti_{2-x}V_x(PO_4)_3$ (where x = 0.5, 0.1, and 0.15) have been synthesized using a traditional solid-state reaction technique. X-ray diffraction (XRD) patterns of the LTP samples heat-treated at 1150 °C for 2 h demonstrated that a phase-pure LTP with rhombohedral symmetry and space group *R3c* (167) was formed. The introduction of vanadium into the LTP resulted in a noticeable shift of high-intensity bands towards lower wavenumbers, along with an enhancement in the peak intensities at 492 and 486 cm^{-1} in the Raman spectra. Scanning electron microscope (SEM) images revealed an increase in grain size as the vanadium content rose. At room temperature, the highest ionic conductivity was found to be 0.82×10^{-4} S/cm for the composition of x = 0.15. Conductivity investigations indicated that the sample with V (x = 0.15) exhibited higher conductivity when compared to those with 0.05 and 0.10. The conductivity measured for V (x = 0.05, 0.10 and 0.15) at low operating temperatures ranging from 150 to 350 °C were also measured and found to be higher for sample x = 0.15 as 0.92×10^{-2} S/cm at 350° C. The vanadium-substituted $LiTi_2(PO_4)_3$ solid electrolyte exhibits superior structural

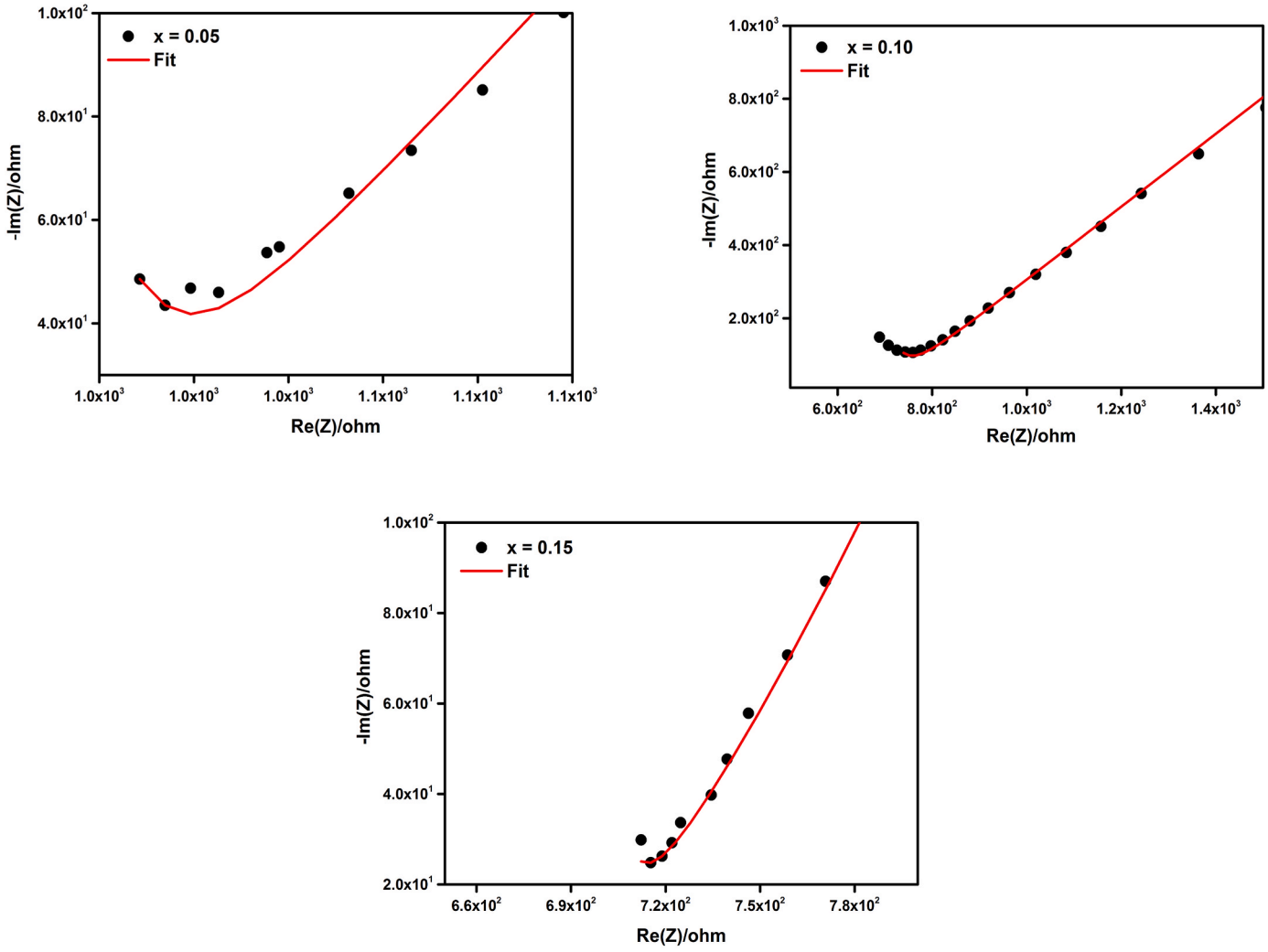


Fig. 5 (c). Nyquist plots of V doped LTP at x = 0.05, 0.10 and 0.15 electrolytes measured at 350° C operating temperature.

Table 2
Conductivity values of LTP & V doped LTP for x = 0.05, 010 and 0.15 at room temperature.

Electrolyte	Room temperature (Scm^{-1})
LTP (x = 0.0)	0.71×10^{-5}
LVTP (x = 0.05)	0.59×10^{-5}
LVTP (x = 0.10)	0.27×10^{-5}
LVTP (x = 0.15)	0.82×10^{-4}

and electrochemical properties compared to the pristine LTP. The incorporation of V^{5+} ions enhances lithium-ion mobility by generating additional Li^{+}vacancies, resulting in significantly improved ionic conductivity and thermal stability. The optimized composition demonstrates excellent phase stability, reduced grain boundary resistance, and reliable performance even at elevated temperatures. These outstanding features confirm vanadium-substituted LTP as a highly promising solid electrolyte material for next-generation lithium-ion batteries. Some common solid electrolytes for lithium-ion batteries include: NASICON-type materials: e.g., $LiTi_2$ $(PO_4)_3$ (LTP), $Li_{1+x}Al_xTi_{2-x}(PO_4)_3$ (LATP), Garnet-type: e.g., $Li_7La_3Zr_2O_{12}$ (LLZO), Sulfide-based: e.g., $Li_{10}GeP_2S_{12}$ (LGPS) and Polymer electrolytes: e.g., PEO-Li salts. LTP (pure) electrolytes exhibit conductivity range of about 10^{-4}–10^{-3} at RT–100 °C. Here, in the present work Vanadium-doped LTP exhibits a conductivity of about 0.82×10^2 (RT), 0.92×10^2 (350 °C) RT – 350 °C which indicates

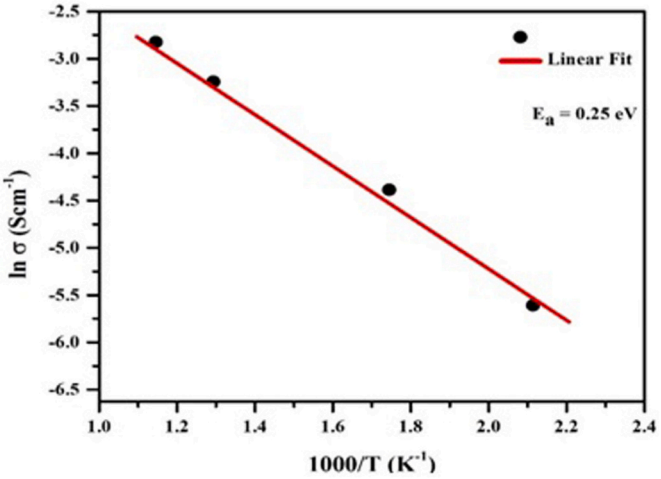


Fig. 6. Arrhenius plot of V doped LTP at x = 0.15 electrolytes measured at operating temperatures from 50 to 350° C.

high Enhanced conductivity, high-temp stability. Other commonly used electrolyte such as LATP provides ~10^{-3} RT Moderate High conductivity, LLZO ~10^{-3} RT Excellent High ionic conductivity and LGPS

Table 3
Conductivity values of V doped LTP for x = 0.05, 0.10 and 0.15 at various temperatures.

Electrolyte	150° C (Scm^{-1})	250° C (Scm^{-1})	350° C (Scm^{-1})
LVTP 0.05	0.21×10^{-5}	0.12×10^{-4}	0.24×10^{-3}
LVTP 0.10	0.84×10^{-4}	0.87×10^{-3}	0.19×10^{-3}
LVTP 0.15	0.36×10^{-4}	0.71×10^{-3}	0.91×10^{-2}

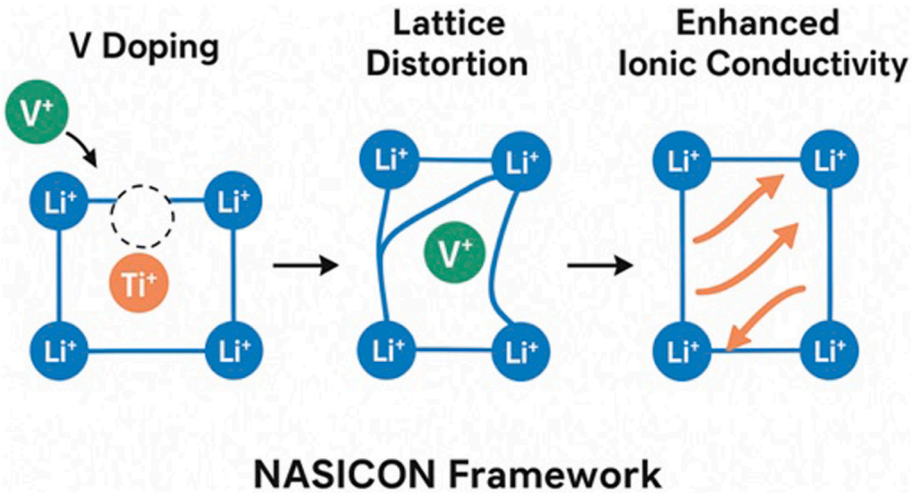


Fig. 7. Representation of the lattice distortion leading to enhanced ionic conductivity on vanadium doping in the LTP structure.

$\sim 10^{-2}$ RT Moderate Very high conductivity. Compared to mainstream solid electrolytes, the vanadium-doped LTP demonstrates significantly enhanced ionic conductivity at both room and elevated temperatures. While garnet-type LLZO and sulfide-based LGPS offer high ionic conductivity at room temperature, they often require complex synthesis routes or exhibit lower thermal stability. The vanadium-doped LTP provides a balance of high conductivity, thermal stability, and simpler synthesis, making it a promising candidate for high-performance lithium-ion batteries.

CRediT authorship contribution statement

A. Panneerselvam: Writing – original draft, Methodology, Investigation. **V.M. Senthilkumar:** Methodology, Investigation, Conceptualization. **R. Senthil kumar:** Methodology, Investigation, Conceptualization. **S. Satheeskumar:** Methodology, Investigation, Conceptualization. **S. Selvakumar:** Validation, Methodology, Investigation, Conceptualization, Formal analysis, Writing – review & editing. **S.C. Vella Durai:** Writing – review & editing, Methodology, Investigation, Formal analysis, Writing – original draft, Visualization.

Funding

This research received no funding.

Declaration of competing interest

The authors declare the following financial interests/personal relationships which may be considered as potential competing interests: Dr. A. Panneerselvam reports administrative support and statistical analysis were provided by A. Panneerselvam Department of Physics, Vivekanandha College of Engineering for Women (Autonomous), Tiruchengode, Namakkal - 637 205, Tamil Nadu, India. Dr. A. Panneerselvam reports a relationship with Department of Physics, Vivekanandha College of Engineering for Women (Autonomous), Tiruchengode, Namakkal - 637 205, Tamil Nadu, India that includes: employment. Dr. A. Panneerselvam has patent pending to NIL. NIL If there are other authors, they declare that they have no known competing financial interests or personal relationships that could have appeared to influence the work reported in this paper.

Data availability

No data was used for the research described in the article.

References

[1] N.V. Kosova, D.I. Osintsev, N.F. Uvarov, E.T. Devyatkna, Lithium titanium phosphate as cathode, anode and electrolyte cyclic voltamograms for $LiTi_{2-x}Nb_x(PO_4)_3$ with (x = 0, 0.05, 0.075,0.1 and 0.15, Chem. Sustain. Dev. 13 (2005) 253–260.
[2] Z. Cheng, T. Liu, B. Zhao, F. Shen, H. Jin, X. Han, Recent advances in organic-inorganic composite solid electrolytes fo r all-solid-state lithium batteries, Energy Storage Mater. 34 (2021) 388–416, https://doi.org/10.1016/j.ensm.2020.09.016.
[3] V. Thangadurai, K. Ashok, J. Gopala Krishnan, New lithium – ion conductors based on the NASICON structure, J. Mater. Chem. 9 (1999) 739–741, https://doi.org/10.1039/A807007E.
[4] M.J. Lee, J. Han, K. Lee, Y.J. Lee, B.G. Kim, K.N. Jung, B.J. Kim, S.W. Lee, Elastomeric electrolytes for high-energy solid-state lithium batteries, Nature 601 (2022) 217–222, https://doi.org/10.1038/s41586-021-04209-4.
[5] J.B. Goodenough, H.Y.P. Hong, J.A. Kafalas, Fast Na^+ -ion transport in skeleton structures, Mater. Res. Bull. 11 (1976) 203–220, https://doi.org/10.1016/0025-5408(76)90077-5.
[6] S. Chen, K. Wen, J. Fan, Y. Bando, D. Golberg, Progress and future prospects of high-voltage and high-safety electrolytes in advanced lithium batteries: from liquid to solid electrolytes, J. Mater. Chem. A 6 (2018) 11631–11663, https://doi.org/10.1039/C8TA03358G.
[7] A. Orliukas, A. Dindune, Z. Kanepe, J. Ronis, E. Kazakevicius, A. Kežionis, Synthesis, structure and peculiarities of ionic transport of $Li_{1.6}Mg_{0.3}Ti_{1.7}(PO_4)_3$ ceramics, Solid State Ionics 157 (2003) 177–181, https://doi.org/10.1016/S0167-2738(02)00206-0.
[8] L. Sun, Y. Wang, L. Kong, S. Chen, C. Peng, J. Zheng, Y. Li, W. Feng, Designing mesostructured iron (II) fluorides with a stable in situ polymer electrolyte interface for high-energy-density lithium-ion batteries, eScience 4 (2024) 100188, https://doi.org/10.1016/j.esci.2023.100188.
[9] H. Aono, M.A. Idris, Y. Sadaoka, Ionic conductivity and crystal structure for the $Li_{3-2x}Cr_{2-x}Ta_x(PO_4)_3$, Solid State Ionics 166 (2004) 53–59, https://doi.org/10.1016/j.ssi.2003.11.005.
[10] G.X. Wang, D.H. Bradhurst, S.X. Dou, H.K. Liu, $LiTi_2(PO_4)_3$ with NASICON- type structure as lithium –storage materials, J. Power Sources 124 (2003) 231–236, https://doi.org/10.1016/S0378-7753(03)00609-8.

[11] C. Sangeland, T. Tjessem, J. Mindemark, D. Brandell, Overcoming the obstacle of polymer–polymer resistances in double layer solid polymer electrolytes, J. Phys. Chem. Lett. 12 (2021) 2809–2814, https://doi.org/10.1021/acs.jpclett.1c00366.
[12] I.Y. Pinus, I.A. Stenina, A.I. Rebrov, N.A. Zhuravlev, A.B. Yaroslavtsev, Cation mobility inmodified $Li_{1-x}Ti_{2-x}Nb_x(PO_4)_3$ lithium titanium NASICON phosphates, Russsian J. Inorg. Chem. 54 (2009) 1177–1180, https://doi.org/10.1134/S0036023609080026.
[13] N. Guo, Z. Peng, W. Huo, Y. Li, S. Liu, L. Kang, X. Wu, L. Dai, L. Wang, S.C. Jun, Z. He, Stabilizing Zn metal anode through regulation of Zn ion transfer and interfacial behavior with a fast ion conductor protective layer, Small 19 (2023) 2303963, https://doi.org/10.1002/smll.202303963.
[14] P. Maldonado- Manso, E.R. Losilla, M.M. Lara, M.A.G. Aranda, S. Bruque, F. E. Mouahid, M. Zhair, High lithium ionic conductivity in the Li_{1+x} $Al_xGe_yTi_{2-x-y}$ $(PO_4)_3$ NASICON series, Chem. Mater. 15 (2003) 1879–1885, https://doi.org/10.1021/cm021717j.
[15] Y. Liu, Y. Zhu, Y. Cui, Challenges and opportunities towards fast-charging battery materials, Nat. Energy 4 (2009) 540–550, https://doi.org/10.1038/s41560-019-0405-3.
[16] G.F. Ortiz, M.C. Lopez, P. Lavela, C. Vidal-Abarca, J.L. Tirado, Improved lithium–ion transport in NASICON –type lithium titanium phosphate by calcium and iron doping, Solid State Ionics 262 (2013) 573–577, https://doi.org/10.1016/j.ssi.2013.09.012.
[17] M.R. Shaik, M. Bissannagari, Y.M. Kwon, K.Y. Cho, J. Kim, S. Yoon, Soft, robust, Li-ion friendly halloysite-based hybrid protective layer for dendrite-free Li metal anode, Chem. Eng. J. 424 (2021) 130326, https://doi.org/10.1016/j.cej.2021.130326.
[18] T. Savitha, S. Selva Sekara Pandian, C.S. Ramya, M.S. Bhuvaneswari, P.C. Angelo, Electrical conduction and relaxation mechanism in Li_2AlZr $[PO_4]_3$, J. Mater. Sci. 4 (2007) 5470–5475, https://doi.org/10.1007/s10853-006-0983-x.
[19] J. Li, C. Ma, M. Chi, C. Liang, N.J. Dudney, Solid electrolyte: the key for high-voltage lithium batteries, Adv. Energy Mater. 5 (2015) 1401408, https://doi.org/10.1002/aenm.201401408.
[20] S. Kim, J.S. Kim, L. Miara, Y. Wang, S.K. Jung, S.Y. Park, Z. Song, H. Kim, M. Badding, J. Chang, V. Roev, G. Yoon, R. Kim, J.H. Kim, K. Yoon, D. Im, K. Kang, High-energy and durable lithium metal batteries using garnet-type solid electrolytes with tailored lithium-metal compatibility, Nat. Commun. 13 (2022) 1833, https://doi.org/10.1038/s41467-022-29531-x.
[21] Q. Liu, Q. Yu, S. Li, S. Wang, L. Zhang, B. Cai, D. Zhou, B. Li, Safe LAGP-based all solid-state Li metal batteries with plastic super-conductive interlayer enabled by insitu solidification, Energy Storage Mater. 25 (2020) 613–620, https://doi.org/10.1016/j.ensm.2019.09.023.
[22] Y. Zheng, Y. Yao, J. Ou, M. Li, D. Luo, H. Dou, Z. Li, K. Amine, A. Yu, Z. Chen, A review of composite solidstate electrolytes for lithium batteries: fundamentals, key materials and advanced structures, Chem. Soc. Rev. 49 (2020) 8790–8839, https://doi.org/10.1039/D0CS00305K.
[23] M.R. Shaik, M.J. Yeo, K.Y. Cho, S. Yoon, Robust artificial HfO_2/PEDOT: PSS polarity layer for increasing stability of Li metal anodes, J. Alloys Compd. 939 (2023) 168703, https://doi.org/10.1016/j.jallcom.2023.168703.
[24] S. Wang, Q.X. Shi, Y.S. Ye, Y. Wang, H.Y. Peng, Z.G. Xue, X.L. Xie, Y.W. Mai, Polymeric ionic liquid-functionalized mesoporous silica nanoplates: a new high performance composite polymer electrolyte for lithium batteries, Electrochim. Acta 245 (2017) 1010–1022, https://doi.org/10.1016/j.electacta.2017.05.125.
[25] M.R. Shaik, Y. Park, Y.K. Jung, W.B. Im, Interfacial modulation of bi functional electrolyte additive engineering for dendrite-free and robust lithium metal anode, J. Energy Chem. 97 (2024) 120–127, https://doi.org/10.1016/j.jechem.2024.05.036.
[26] Shalu, V.K. Singh, R.K. Singh, Development of ion conducting polymer gel electrolyte membranes based on polymer PVdF-HFP, BMIMTFSI ionic liquid and the Li-salt with improved electrical, thermal and structural properties, J. Mater. Chem. C 3 (2015) 7305–7318, https://doi.org/10.1039/C5TC00940E.
[27] S. Han, J.H. Lee, J. Kim, J. Lee, Recent advances in li metal anode protection for high performance lithium-sulfur batteries, Discov. Chem. Eng. 4 (2024) 9, https://doi.org/10.1007/s43938-024-00045-w.
[28] F. Zheng, M. Kotobuki, S. Song, M.O. Lai, L. Lu, Review on solid electrolytes for all-solid-state lithium-ion batteries, J. Power Sources 389 (2018) 198–213, https://doi.org/10.1016/j.jpowsour.2018.04.022.
[29] G.P. Pandey, S.A. Hashmi, Experimental investigations of an ionic-liquid-based, magnesium ion conducting, polymer gel electrolyte, J. Power Sources 187 (2009) 627–634, https://doi.org/10.1016/j.jpowsour.2008.10.112.
[30] Q. Liu, X. Zhao, Q. Yang, L. Hou, D. Mu, G. Tan, L. Li, R. Chen, F. Wu, The progress in the electrolytes for solid state sodium-ion battery, Adv. Mater. Technol. 8 (2023) 2200822, https://doi.org/10.1002/admt.202200822.
[31] I. Osada, H. de Vries, B. Scrosati, S. Passerini, Ionic-liquid-based polymer electrolytes for battery applications, Angew. Chem. Int. Ed. 55 (2016) 500–513, https://doi.org/10.1002/anie.201504971.
[32] L. Li, E. Han, L. Zhu, S. Qiao, C. Du, H. Liu, Effect of Zr doping and Al-Zr co-doping on LiNi0.5Co0.25Mn0.25O2 for lithium-ion batteries, Solid State Ionics 346 (2020) 115220, https://doi.org/10.1016/j.ssi.2019.115220.
[33] V. Shukla, K. Balani, A. Subramaniam, S. Omar, Phase stability and conductivity in the pseudo ternary system of $xYb_2O_3.(12.{}_x)Sc_2O_{3\text{-}88}ZrO_2$ ($0 \leq x \leq 5$), Solid State Ionics 332 (2019) 93–101, https://doi.org/10.1016/j.ssi.2019.01.005.